Unlocking the Constraints of Cyanobacterial Productivity: Acclimations Enabling Ultrafast Growth

Hans C. Bernstein,[a,b,h] Ryan S. McClure,[b] Eric A. Hill,[b] Lye Meng Markillie,[c] William B. Chrisler,[b] Margie F. Romine,[b] Jason E. McDermott,[b] Matthew C. Posewitz,[d] Donald A. Bryant,[e,f] Allan E. Konopka,[b,g] James K. Fredrickson,[b] Alexander S. Beliaev[b]

Chemical and Biological Signature Science, Pacific Northwest National Laboratory, Richland, Washington, USA[a]; Biological Sciences Division, Pacific Northwest National Laboratory, Richland, Washington, USA[b]; Environmental Molecular Sciences Laboratory, Pacific Northwest National Laboratory, Richland, Washington, USA[c]; Department of Chemistry and Geochemistry, Colorado School of Mines, Golden, Colorado, USA[d]; Department of Biochemistry and Molecular Biology, The Pennsylvania State University, University Park, Pennsylvania, USA[e]; Department of Chemistry and Biochemistry, Montana State University, Bozeman, Montana, USA[f]; Department of Biological Sciences, Purdue University, West Lafayette, Indiana, USA[g]; The Gene and Linda Voiland School of Chemical Engineering and Bioengineering, Washington State University, Pullman, Washington, USA[h]

ABSTRACT Harnessing the metabolic potential of photosynthetic microbes for next-generation biotechnology objectives requires detailed scientific understanding of the physiological constraints and regulatory controls affecting carbon partitioning between biomass, metabolite storage pools, and bioproduct synthesis. We dissected the cellular mechanisms underlying the remarkable physiological robustness of the euryhaline unicellular cyanobacterium *Synechococcus* sp. strain PCC 7002 (*Synechococcus* 7002) and identify key mechanisms that allow cyanobacteria to achieve unprecedented photoautotrophic productivities (~2.5-h doubling time). Ultrafast growth of *Synechococcus* 7002 was supported by high rates of photosynthetic electron transfer and linked to significantly elevated transcription of precursor biosynthesis and protein translation machinery. Notably, no growth or photosynthesis inhibition signatures were observed under any of the tested experimental conditions. Finally, the ultrafast growth in *Synechococcus* 7002 was also linked to a 300% expansion of average cell volume. We hypothesize that this cellular adaptation is required at high irradiances to support higher cell division rates and reduce deleterious effects, corresponding to high light, through increased carbon and reductant sequestration.

IMPORTANCE Efficient coupling between photosynthesis and productivity is central to the development of biotechnology based on solar energy. Therefore, understanding the factors constraining maximum rates of carbon processing is necessary to identify regulatory mechanisms and devise strategies to overcome productivity constraints. Here, we interrogate the molecular mechanisms that operate at a systems level to allow cyanobacteria to achieve ultrafast growth. This was done by considering growth and photosynthetic kinetics with global transcription patterns. We have delineated putative biological principles that allow unicellular cyanobacteria to achieve ultrahigh growth rates through photophysiological acclimation and effective management of cellular resource under different growth regimes.

It has long been established that photoautotrophic growth is dependent on the combined rates of light, carbon, and macronutrient acquisition and the efficiencies by which these resources are directed toward biomass synthesis (1). The inherent differences between the rates of light and dark processes highlight an important paradigm that defines cyanobacterial productivity constraints, whereby photosynthetic energy acquisition and CO_2 fixation are interdependent but maintain distinct enzymatic mechanisms and kinetics (2, 3). Under high irradiances, photosynthesis is adversely affected by damage (photoinhibition) to the light-harvesting machinery (1) and/or by photorespiration as RuBisCO selectivity shifts toward O_2 (4). Notably, most of what is known about these effects as a function of irradiance and O_2 tension concerns photosynthesis (5–7) rather than cell growth.

The typical range of doubling times for well-characterized unicellular cyanobacteria (e.g., *Synechocystis* sp. strain PCC 6803 and *Synechococcus elongatus* PCC 7942) is between 7 and 12 h (8, 9). Several hypotheses concerning mechanisms constraining cyanobacterial growth rates have been proposed; these include spatial restrictions within the cell that limit diffusion processes (10) as well as metabolic costs that determine partitioning of cellular resources and resulting fitness (11, 12). The optimization model, developed to simulate the partitioning of material and energy within a photoautotrophic cell (11), has extended the concept of growth as a function of proteome allocation between adaptation to niche-specific environments and cell division resources. An important implication of this is the ability to minimize the requirement for niche-adaptive responses that may be a key for cyano-

bacteria to redirect energy and nutrients efficiently toward the biosynthesis of biomass (13). This also holds significance for understanding regulatory switches governing central metabolism and secondary biosynthetic pathways, which are primary targets for bioengineering of cyanobacteria (14, 15).

In this study, we systematically dissected the growth and photophysiological performance of *Synechococcus* sp. strain PCC 7002 (hereafter *Synechococcus* 7002), a fast-growing euryhaline unicellular cyanobacterium (16) that has become a promising biotechnological platform (17–20). Although the physiological behavior of *Synechococcus* 7002 has been investigated under a wide range of irradiance, temperature, and salinity conditions (1, 9, 21–23), there is still a paucity of information concerning principles underlying cyanobacterial growth efficiency and robustness. The photosynthetic potential, thresholds of inhibition, and growth are not explicitly equivalent, and significant variation is expected between different environments (24). Herein, we compared the growth and photosynthetic rates of *Synechococcus* 7002 across varied incident irradiance and dissolved O_2 with a slower growing unicellular cyanobacterium, *Cyanothece* sp. strain ATCC 51142 (hereafter *Cyanothece* 51142) (25). *Cyanothece* 51142 was chosen as a comparative organism because it is a well-characterized strain that is amenable to continuous cultivation (15, 17, 26). The growth rates of *Cyanothece* 51142 are similar, compared to those displayed by other model cyanobacterial strains, such as *Synechocystis* strain 6803, and *Synechococcus elongatus* strain 7942 (8, 9). The irradiance-dependent response was further investigated through global RNA sequencing analysis to correlate the ultrafast growth with the photophysiological dynamics and gene expression of *Synechococcus* 7002. Through integration of state-of-the-art cultivation with photophysiological kinetic analyses and transcriptomic measurements, this genome study provides a new level of insight into the mechanisms guiding the energy and resource partitioning in cyanobacteria and sheds light on the phenomenon of ultrafast photoautotrophic growth.

RESULTS

Ultrafast growth under high irradiance. Optically thin (optical density at 730 nm [OD_{730}] of 0.082 ± 0.003) cultures of *Synechococcus* 7002 and *Cyanothece* 51142 were grown under turbidostat control to maintain nutrient-replete steady states operating at the maximum specific growth rate obtainable for a given environmental condition (27, 28). Under these conditions, *Synechococcus* 7002 displayed specific growth rates (μ) that increased with irradiance to a maximum value of 0.20 ± 0.01 h^{-1}. Growth was not inhibited even at the highest incident irradiance (I_i), 760 μmol photons · m^{-2} · s^{-1}, examined in this study (Fig. 1A). In contrast, specific growth rates for *Cyanothece* 51142 reached a maximum of 0.07 ± 0.01 h^{-1} at 430 μmol photons · m^{-2} · s^{-1} and then declined at higher irradiances. The μ-I_i relationships displayed saturating and/or peak functional trends similar to typical photosynthesis-to-irradiance (P-I) curves (see Fig. S1 in the supplemental material) (29, 30).

The steady-state net specific rates of photosynthesis (q_{O_2}) followed a similar increase as μ (Fig. 1B). Net O_2 production by *Synechococcus* 7002 reached and sustained a maximum value of 9.1 ± 0.2 mmol O_2 · h^{-1} · g$_{AFDW}$$^{-1}$ (AFDW stands for ash-free weight [dry weight]), while *Cyanothece* 51142 cultures peaked at 2.8 ± 0.1 mmol O_2 · h^{-1} · g$_{AFDW}$$^{-1}$ and subsequently decreased at higher irradiances. These results confirm that unlike *Synechococ-*

cus 7002, *Cyanothece* 51142 is susceptible to photoinhibition during steady-state growth at I_i of >430 μmol photons · m^{-2} · s^{-1}. The observed effects on growth occurred at low dissolved O_2 concentrations (≤8.0 and ≤2.5 μM for *Synechococcus* 7002 and *Cyanothece* 51142, respectively).

Based on the growth and photosynthetic relationships with I_i, the physiological responses can be categorized into two distinguishable regimes: (i) a "light-limited" regime, characterized by an increasing linear response to I_i; and (ii) a "light-saturated" regime, which varied from asymptotic growth in *Synechococcus* 7002 to inhibition in *Cyanothece* 51142. The two regimes were separated by a "transitional" phase defined here as the responses at or near the theoretical saturating irradiance I_k (31). The observed bimodal behavior was further supported by net growth-to-photosynthesis yields that are proxies for the photosynthetic quotient (Q) (Cmmol biomass/mmol of O_2), which was defined here as the ratio of the net rate of carbon fixation into biomass to the net rate of oxygenic photosynthesis. For *Synechococcus* 7002, the photosynthetic quotients were higher during light-limited growth (Q_{lim} = 1.3 ± 0.3) than light-saturated growth (Q_{sat} = 0.6 ± 0.1) (Fig. 1C). In contrast, the Q values calculated for growth of *Cyanothece* 51142 varied only from 1.3 ± 0.2 to 1.1 ± 0.4 during light-limited and light-saturated conditions, respectively (Fig. 1D). These results show that Q is greatest during light-limited growth of *Synechococcus* 7002 and also indicate that more reductant is required to support fast growth at higher incident irradiances. The same cannot be concluded for *Cyanothece* 51142, as much slower (≥3-fold) growth rates are supported by an effectively constant amount of net oxygenic photosynthesis regardless of whether I_i is limiting or saturating (i.e., inhibiting) relative to growth.

Photosynthetic performance as a function of growth phase and irradiance. Interrogation of the photosynthetic apparatus via chlorophyll (chlorophyll *a* [Chl *a*]) fluorescence techniques identified further differences between how *Synechococcus* 7002 and *Cyanothece* 51142 acclimate to increasing irradiance. As a general trend, the parameters associated with photosystem performance and photosynthetic electron transfer demonstrated distinct bimodal distributions as a function of light availability (i.e., limited versus saturated regimes). The most remarkable difference between *Synechococcus* 7002 and *Cyanothece* 51142 was the contrasting trends of cyclic electron flow (rate of cyclic electron transport [rCEF]), determined by postillumination fluorescence (Fig. 2A). *Synechococcus* 7002 displayed a positive rCEF rate trend across all I_i values, with the exception of the highest illumination (760 μmol photons · m^{-2} · s^{-1}). In contrast, the rCEF rates in *Cyanothece* 51142 followed both growth and photosynthetic trends and displayed three distinct phases: a fast increase in rCEF associated with light-limited growth (I_i < 430 μmol photons · m^{-2} · s^{-1}), deceleration during the transition I_k (~430 μmol photons · m^{-2} · s^{-1}), and steep decline under light-saturated conditions (I_i > 430 μmol photons · m^{-2} · s^{-1}) associated with inhibition of growth and photosynthesis.

The maximum relative rate of electron transport (rETR$_{max}$) (Fig. 2B) shifted from a positive trend to a negative trend at the transition from light-limited to light-saturated growth for both cyanobacteria. This result indicates that the photosynthetic potential increased with increasing growth under light-limited regimes but leveled off and even decreased under light-saturated growth. Notably, the rETR$_{max}$ values measured in *Synechococcus*
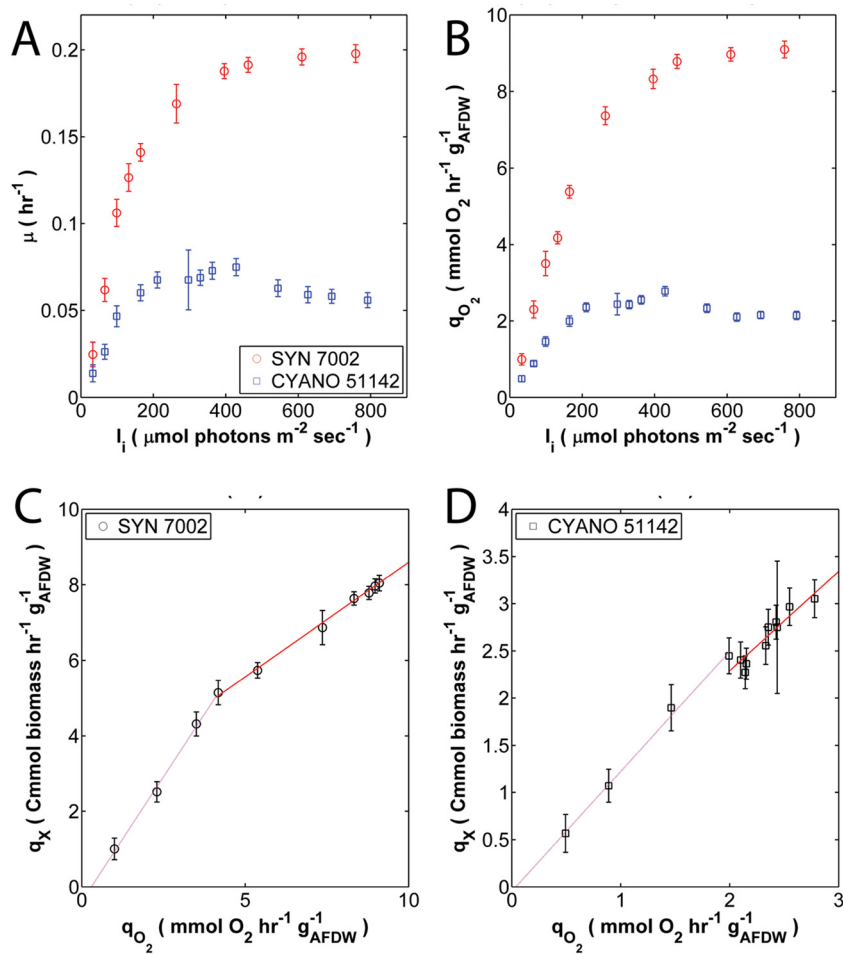
FIG 1 Steady-state growth and photosynthesis values of *Synechococcus* 7002 and *Cyanothece* 51142 controlled at different incident irradiances. (A) Specific growth rates of *Synechococcus* 7002 (SYN 7002) (red circles) and *Cyanothece* 51142 (CYANO 51142) (blue squares). (B) Net specific O_2 production rates (i.e., net oxygenic photosynthesis) of *Synechococcus* 7002 and *Cyanothece* 51142. (C and D) Net specific rates of biomass production on a carbon mole basis (q_X) plotted against the net oxygenic photosynthesis (q_{O_2}) for *Synechococcus* 7002 (C) and *Cyanothece* 51142 (D). The slopes represent the net growth-to-photosynthesis yield (Q) corresponding to either the light-limited phase (pink line) or the light-saturated phase (red line). Values are means ± 1 standard deviation (error bars).

7002 were approximately 3-fold higher than those displayed by *Cyanothece* 51142. Furthermore, the relative maximal quantum yield of photochemistry (α_r) was the highest during light-limited growth and decreased with increasing I_i for both cyanobacteria (Fig. 2C). It should be noted that some of the photosynthesis parameters measured for *Synechococcus* 7002 (e.g., rCEF and α_r)

during the steady state corresponding to the highest I_i (760 μmol photons · m^{-2} · s^{-1}) deviated from the predominant trends observed during light-saturated growth (see Fig. S2 in the supplemental material).

Growth tolerance to increasing O_2 tension. To further define the boundaries of cyanobacterial growth robustness and to simu-
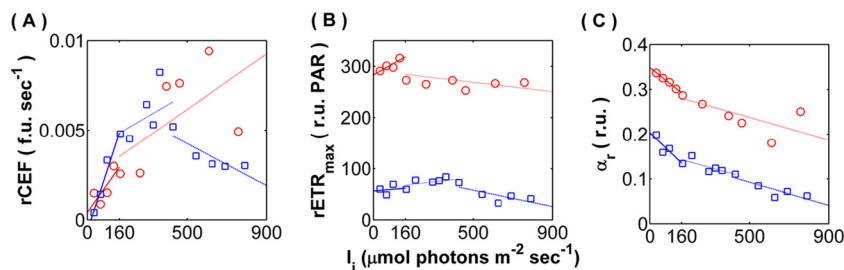

FIG 2 Photosynthesis parameters determined by chlorophyll fluorescence methods. (A) Surrogate rate of cyclic electron flow (rCEF); (B) relative maximum electron transport rate (rETR$_{max}$); (C) relative maximal quantum yield of photochemistry (α_r). Data points specific to *Synechococcus* 7002 and *Cyanothece* 51142 are represented by red circles and blue squares, respectively. Linear regression was used to establish positive or negative trends of each parameter during light-limited growth (solid lines), saturated/peak growth (dotted lines), and photoinhibited growth (dashed lines). f.u., fluorescence units; r.u., relative units.
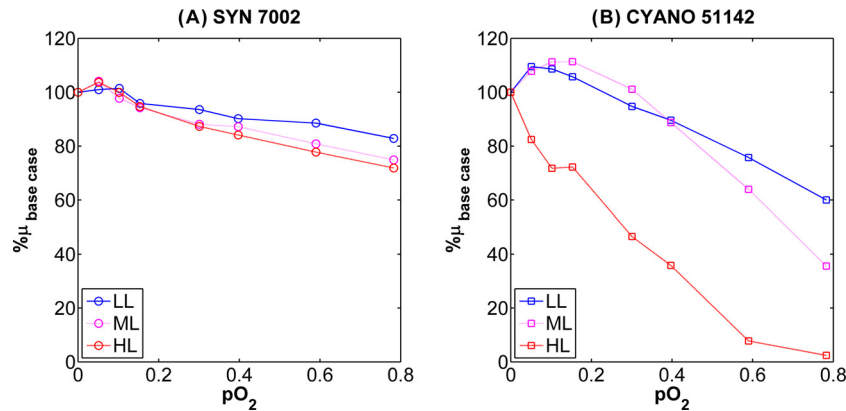
FIG 3 Relative responses of specific growth rate to combinatorial increases in oxygen tension (i.e., partial pressures, pO_2) and incident irradiance. Data are represented as the percent decrease from the baseline growth obtained by sparging the cultures with 2% CO_2 in N_2. (A) *Synechococcus* 7002 oxygen stress profile containing low-light (LL), medium-light (ML), and high-light (HL) conditions corresponding to incident irradiance values of 99, 132, and 760 μmol photons $m^{-2}\,s^{-1}$. (B) *Cyanothece* 51142 oxygen stress profile reporting LL, ML, and HL conditions corresponding to incident irradiance values of 131, 395, and 790 μmol photons $m^{-2}\,s^{-1}$.

late the effects of elevated O_2 tensions that can occur under intense photosynthetic activity, the steady-state turbidostat-grown cultures were subjected to increasing partial O_2 pressure (pO_2). While growth of both *Synechococcus* 7002 (Fig. 3A) and *Cyanothece* 51142 (Fig. 3B) was inhibited by O_2 to a greater degree under high irradiance relative to low irradiance, there were stark differences between the sensitivities of the two organisms to elevated pO_2. *Synechococcus* 7002 was much more resistant to the increasing pO_2 levels, with only a 28% decline in growth rate at a pO_2 of 0.78 (840 μM) and I_i of 760 μmol photons $\cdot$ m^{-2} $\cdot$ s^{-1}. In contrast, the growth rates of *Cyanothece* 51142 decreased severely with increasing O_2 tension under the same irradiance. At a pO_2 of 0.78 and I_i of 760 μmol photons $\cdot$ m^{-2} $\cdot$ s^{-1}, growth of *Cyanothece* 51142 was nearly completely (~98%) inhibited. Interestingly, growth rates for *Cyanothece* 51142 increased in response to increasing pO_2 values up to 0.1 (107 μM), but only at irradiances of <400 μmol photons $\cdot$ m^{-2} $\cdot$ s^{-1}.

Transcriptional responses reveal potential mechanisms of growth robustness. The *Synechococcus* 7002 gene-level responses to light-controlled growth were further interrogated by RNA sequencing. Hierarchical clustering of relative transcript abun-

dances (reads per kilobase per million reads [RPKM]) across a 2,732-gene data set identified four major clusters, whose eigengenes aligned with the growth and photosynthetic performance of *Synechococcus* 7002 across the irradiance scale (Fig. 4; see Table S1 in the supplemental material). Of the four clusters, cluster I contained the largest group of transcripts (29.6%), the relative abundance of which increased in direct proportion with growth rate. Cluster I was functionally enriched ($P < 0.05$) for genes involved in translation (i.e., ribosomal proteins and tRNA aminoacylation), purine biosynthesis, iron-sulfur cluster assembly, and ATP synthesis (Table 1; Table S2). In concert with the putative upregulation of growth-related functions, there was also a broad increase in transcripts involved in amino acid biosynthesis, protein folding, and iron transport and acquisition. Cluster I also contained genes involved in central carbon metabolism reactions such as the anaplerotic pathways containing bifunctional fructose-1,6-bisphosphatase-II/sedoheptulose-bisphosphatase regulated by photosystem I (PS I) activity (32). Furthermore, reflecting an increased demand for CO_2 as an electron sink, the relative mRNA levels of genes of the NADH-plastoquinone oxidoreductase complex involved in CO_2 uptake (*ndhD3*, *ndhF3*, and
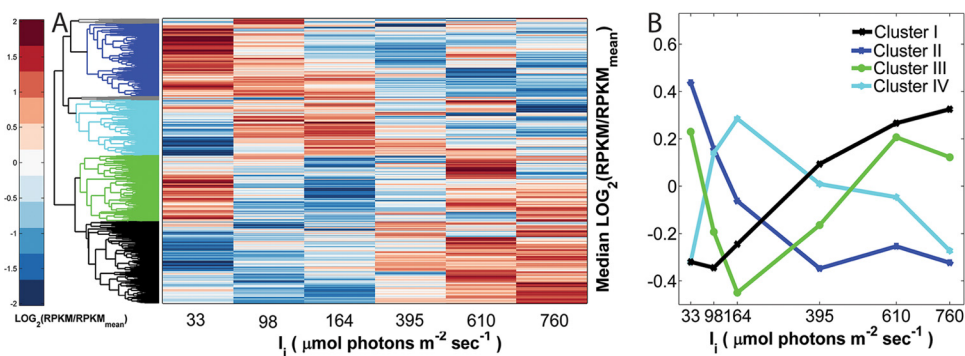
FIG 4 Hierarchical clustering of relative transcript abundances in *Synechococcus* 7002 during steady-state turbidostat growth as a function of incident irradiance. The major clusters of coexpressed genes are color coded as follows. Cluster I genes are shown in black (809 genes), cluster II genes are shown in dark blue (724 genes), cluster III genes are shown in green (648 genes), and cluster IV genes are shown in light blue (551 genes). The full 2,732-gene list of the relative expression values at each steady state is given in Table S1 in the supplemental material. (B) The eigenvector profiles of the four main clusters of differentially expressed genes. The same color coding used for panel A is used for panel B.

TABLE 1 Functional enrichment of irradiance-regulated genes of *Synechococcus* 7002

Role or system and cluster	Functional category	% genes[a]	Ratio[b]	P value[c]
Main role				
I	Translation	13.1	2.5	4.36E−13
I	Amino acid metabolism	5.6	1.8	1.33E−03
II	Cell motility and adherence	1.7	2.6	1.01E−02
IV	Glycan biosynthesis and metabolism	3.8	1.7	3.43E−02
Subrole				
I	Ribosomal proteins: synthesis and modification	6.8	3.1	1.27E−09
I	tRNA biogenesis	2.5	3.3	1.73E−04
I	Iron-sulfur clusters	0.9	3.5	1.89E−02
II	Peptidases	4.0	1.8	1.28E−02
II	Photosynthesis-antenna proteins	1.7	2.2	2.94E−02
II	Surface structures and assembly platforms	1.4	2.5	2.64E−02
III	Plasmid functions	1.4	2.2	4.82E−02
III	RNA degradation	1.2	2.6	4.31E−02
III	Protein modification and repair	0.9	3.0	3.95E−02
III	Riboflavin metabolism	0.8	3.5	3.78E−02
IV	Toxin-antitoxin systems	4.9	1.7	2.54E−02
IV	Two-component systems	3.4	1.7	4.09E−02
IV	Polysacaharide and lipopolysaccharide metabolism	2.7	2.4	7.89E−03
Subsystem				
I	Ribosome large subunit	3.7	3.7	5.13E−07
I	Ribosome small subunit	2.3	3.6	9.03E−05
I	tRNA aminoacylation	2.3	3.6	9.03E−05
I	Purine biosynthesis from ribose-5-phosphate	1.1	2.7	2.80E−02
I	F_1/F_o ATPase AtpABCDEFGH	1.1	3.6	7.02E−03
I	Iron-sulfur cluster assembly SUF system	0.7	3.4	3.13E−02
II	Photosystem II main subunits	1.0	3.4	1.74E−02
II	Photosystem I other common subunits	0.6	4.4	4.32E−02
II	P-type pilus	0.6	4.4	4.32E−02
III	NAD(P)H:quinone oxidoreductase (complex I)	1.9	2.5	1.31E−02
III	High-affinity urea uptake system UrtABCDE	0.6	3.9	4.97E−02
IV	Polysaccharide biosynthesis	3.1	2.9	9.04E−04
IV	Polymorphic toxins	1.8	2.2	3.37E−02
IV	Nickel-dependent hydrogenase	1.8	4.5	8.20E−04
IV	N-type Na translocation ATPase	1.3	4.5	4.91E−03
IV	Glycolipid biosynthesis	0.9	4.8	1.45E−02
IV	Light-independent protochlorophyllide reductase	0.7	5.8	1.98E−02
IV	T2bSS type IVa pilus complex	0.7	3.9	4.67E−02
IV	Pentose phosphate pathway oxidative phase	0.5	5.8	4.49E−02
IV	Polyphosphate kinase/exopolyphosphatase system	0.5	5.8	4.49E−02

[a] The percentage of genes of a given function within a given functional category.
[b] The percentage of a particular functional category within the cluster versus the percentage of genes of that functional category within the genome as a whole.
[c] The P value represents the probability that the number of genes associated with a specific pathway/regulon occurs by chance.

cupS) (33) were elevated in response to increasing irradiance. While not displaying significant functional enrichment within cluster I, the relative transcript abundance of genes involved in peptidoglycan biosynthesis (*mreB* and *mreC*) and cell division (*minCDE*) increased with growth rate. Remarkably, confocal microscopic analysis of *Synechococcus* 7002 turbidostat cultures revealed that the average cell volume changed proportionally with growth rate (Fig. 5). Specifically, the transition of *Synechococcus* 7002 from light-limited ($I_i = 98$ μmol photons $\cdot$ m^{-2} $\cdot$ s^{-1}) to light-saturated growth ($I_i = 395$ μmol photons $\cdot$ m^{-2} $\cdot$ s^{-1}) resulted in doubling of the average cell volume from 4.84 to 9.69 μm³.

Gene expression levels in cluster II, which contained 26% of the total transcripts, were inversely correlated with the growth rate (Fig. 4 and Table 1; see Table S3 in the supplemental material).
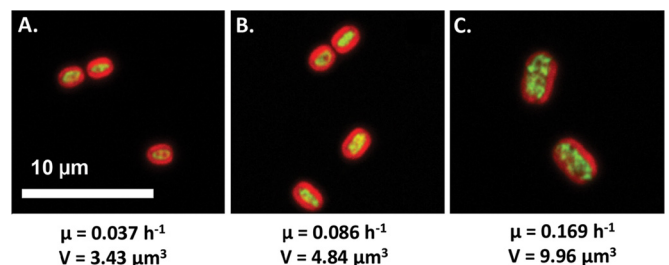

A. μ = 0.037 h⁻¹ V = 3.43 μm³
B. μ = 0.086 h⁻¹ V = 4.84 μm³
C. μ = 0.169 h⁻¹ V = 9.96 μm³

FIG 5 Increase in average cell volumes of *Synechococcus* 7002 cells as a function of irradiance-driven specific growth rates. The volumes were calculated for steady-state cultures grown at I_i values of 66 (A), 98 (B), and 395 (C) μmol photons $\cdot$ m^{-2} $\cdot$ s^{-1} and represent an average of 104, 107, and 65 individual cell measurements, respectively. The cells were visualized by autofluorescence (red) and SYBR gold (green). Micrograph images representative of each condition were standardized by the bar.

This cluster was functionally enriched in genes encoding photosystems I and II antenna proteins and contained most of the critical genes required for photosynthesis. Among other transcripts were those encoding key putative signal transduction and regulatory proteins such as the thioredoxin-responsive regulator of photosynthesis and carbon fixation (*pedR*), the ferric uptake regulator (*fur*), and the positive phototaxis signal transduction system (*pixL-pixGH*), which was downregulated in excess light. Notably, the increase in specific growth rates was associated with a relative decline in transcript abundance of *Synechococcus* 7002 group 2 and 3 RNA polymerase σ factors, which are typically required for the expression of stress-induced pathways or niche-adaptive protein functions (34).

The eigengene profiles of clusters III and IV exhibited minima and maxima, respectively, at the steady state associated with the transition from light-limited to light-saturated growth (I_k of $\approx$164 μmol photons $\cdot$ m^{-2} $\cdot$ $^{-1}$). Cluster III (Fig. 4 and Table 1; see Table S4 in the supplemental material), which contained 23% of the expressed genome, included genes associated with photodamage and stress responses, including PS I and PS II stability and repair. Among the genes displaying increased relative mRNA abundance during light-saturated growth were two carboxysome structural genes (*ccmK2* and *ccmK4*), the carbonic anhydrase gene (*ccaA*), the RuBisCO subunits (*rbcSL*), and the CO_2 fixation transcriptional regulator (*ccmR*). The genes encoding the core subunits of the Ndh-1 complex of *Synechococcus* 7002 (*ndhHIJK* and *ndhA-ndhB-ndhCG*) along with the NdhD1 subunit responsible for cyclic electron transfer around PS I also showed irradiance-dependent increases under light-saturating conditions (33). Cluster IV, containing 20.2% of the transcriptome, exhibited gene expression trends inverse to cluster III; its eigengene displayed increase under light-limiting conditions and then decreased for each successive steady state within the light-saturated regime (Fig. 4, Table 1, and Table S5). Cluster IV was functionally enriched for polysaccharide and glycolipid biosynthesis, the oxidative branch of the pentose phosphate pathway, nickel-iron hydrogenase biogenesis, and genes involved in electron transport processes such as cyclic electron flow at low light intensities (*psaE*) (35) and oxidative phosphorylation (*coxAB* and *sucC*). While many of these pathways can serve as potential reductant sinks (36), they were downregulated under light-saturating conditions, suggesting the presence of alternative mechanisms of reductant partitioning and oxidative stress mitigation in *Synechococcus* 7002.

DISCUSSION

This study yields insight into an important biological principle, which allows unicellular cyanobacteria to achieve ultrafast growth by having ultrahigh growth rates and manage cellular resource under different irradiance-controlled growth regimes. Herein, we provide direct evidence that the bimodal transition around the theoretical saturating irradiance (I_k) extends not only to the adjustment of the photosynthesis and growth rates but is also coupled to regulation of specific metabolic reactions and cellular functions. The mechanisms by which *Synechococcus* 7002 mitigates the negative effects of high irradiance that typically inhibit the growth and photosynthesis processes of unicellular cyanobacteria are likely to have broader implications for understanding the metabolic and regulatory underpinnings of photosynthetic growth (2, 3).

Consistent increases in relative transcript abundance with in-

creasing irradiance was observed for genes encoding translational machinery, amino acid and nucleotide biosynthesis, the ATPase complex, and the anaplerotic pathways of central carbon metabolism (Fig. 4, cluster I; see Table S2 in the supplemental material). At the same time, the irradiance-driven increase in the relative growth rate of *Synechococcus* 7002 coincided with the broad decrease in transcripts encoding light acquisition machinery and photosystem I and II reaction centers. These coupled transcriptional responses suggest that the level of resources expended for biomass (i.e., protein synthesis) and energy (ATP) synthesis continue to increase with irradiance, while biomass production and net photosynthesis rates are essentially constant due to increased resource expenditure required.

Furthermore, our data provide direct experimental support to earlier calculations (11) positing that energy demand increases to sustain growth, even when growth is light saturated, across increasing irradiance inputs. Reduced net growth-to-photosynthesis yields ($Q_{lim} > Q_{sat}$) during light-replete steady states (Fig. 2) confirm that, while *Synechococcus* 7002 growth is not inhibited at the high-I_i treatments, the ratio of biomass production to energy acquisition decreases once irradiance exceeds an optimum observed near I_k. This is most likely due to the decrease in the optical cross section of the photosynthetic apparatus, as *Synechococcus* 7002 transitions from light-limited to light-saturated growth (1). This transition has negative effects upon the quantum efficiencies of PS II, and in other oxygenic phototrophs, it is linked to increased photoinhibition. Here, we suggest that the reduction in antenna size also allows the cells to redirect carbon and energy fluxes toward biosynthetic processes which fuel cell division. Notably, this metabolic redistribution in *Synechococcus* 7002 occurs in conjunction with a tripling in average cell volume (Fig. 5), a physiological phenomenon that is known to also occur in heterotrophic organisms (i.e., *Salmonella enterica* serotype Typhimurium) in response to increased rate of division (37). These increases in cell mass and size are thought to accommodate the changes in the number of nuclei/cell and can relieve molecular crowding that limits cell growth (11). To that end, removing physical constraints may increase the intracellular capacity needed to accommodate the biosynthetic machinery supporting higher growth rates and alleviate photoinhibition through increased reductant sequestration capacities.

This mechanistic concept is further corroborated by the absence of observed photoinhibition within the *Synechococcus* 7002 steady states (Fig. 3), as increases in irradiance correlated with the generally decreased mRNA levels of known light-sensitive photosystem reaction centers (*psbAD* and *psaAB*). Interestingly, *Synechococcus* 7002 may be unusual, as the lack of elevated transcription of *psb* genes under increasing irradiance contrasts with other transcriptional studies of various slower-growing cyanobacteria exposed to differential and/or stress-inducing light regimes (38–42). The signatures of PS II inhibition were also not observed in the Chl *a* fluorescence analyses performed on *Synechococcus* 7002 (data not shown). For example, the relative maximum rate of electron transport (rETR$_{max}$) increased through the light-limited regime and showed no significant change during light-saturated steady-state growth (transitional saturated states). Furthermore, the regulation of genes mediating reactive oxygen species (ROS) scavenging does not occur uniformly at the transcriptional level. This is consistent with previous gene expression studies (23, 43, 44), which suggested that lack of strong concerted upregulation of

stress response machinery under high irradiance levels may reflect other mechanisms employed by *Synechococcus* 7002 for dealing with excess reductant to avoid photoinhibition.

A key observation in support of the above conclusion is based on substantially elevated levels of rCEF displayed by *Synechococcus* 7002 under saturating high irradiances (Fig. 2), indicating reduction of the plastoquinone (PQ) pool from electron donors not associated with PS II (22). While the exact mechanisms and role of CEF are not fully understood in cyanobacteria, it is postulated that this process contributes to balancing reductant and ATP pools, especially under low irradiance levels (45). Interestingly, *psaE* and *ndhOP* genes, encoding the PS I subunit and PQ-oxidoreductase, respectively, which were previously implicated in CEF (35, 46), displayed maximum relative expression only during the transitional steady state but were downregulated at saturating irradiances (cluster IV in Table S5 in the supplemental material). In contrast, genes encoding the core subunits of the Ndh-1 complex along with the NdhD1 subunit responsible for cyclic electron transfer around PS I (*ndhHIJK* and *ndhA-ndhB-ndhCG*) showed irradiance-dependent increase in abundance under light-saturating conditions (cluster III in Table S4). Thus, our data implicate new genes (i.e., *ndhHIJK* and *ndhA-ndhB-ndhCG*) with potentially important roles in the cyclic electron transport of *Synechococcus* 7002 that are inherently linked to its ability to effectively partition reductant fluxes and avoid detrimental effects of oxidative stress using multiple strategies.

In summary, a coordinated, functionally grouped gene expression was observed which broadly supports inferences about the role that transcriptional regulation may play in processes such as photosynthesis, carbon fixation, electron transport, and stress response. Interestingly, the kinetics of growth and photosynthesis revealed bimodal growth regimes with respect to carbon uptake to chemical energy production yields, providing evidence of increased cellular energy expenditure during growth at high (but not inhibiting) irradiances. This effect was corroborated by observations that the relative expression of genes involved in biomass synthesis and chemical energy production continued to increase even when the growth and photosynthetic rates were essentially constant, showing strong evidence for an increased energy requirement with increasing light energy input. Only a few other studies have ever demonstrated distinct saturating and/or inhibition kinetics of specific growth rate as a function of irradiance (47–50). Finally, this study sets a bench mark for specific growth rate ($\mu = 0.2\ h^{-1}$) achieved by mesophilic cyanobacteria (16, 43, 51) and provides a foundation for understanding the linkages between photosynthetic performance and growth which can bring fundamental new insights that are broadly applicable to other photosynthetic and nonphotosynthetic biological systems.

MATERIALS AND METHODS

Bacterial cultures and growth. *Synechococcus* sp. strain PCC 7002 and *Cyanothece* sp. strain ATCC 51142 were cultured in modified A-plus medium which contained 17 mM NH_4Cl (52). Starter cultures for the bioreactor were initiated from frozen stocks and were grown as batch cultures in sealed serum bottles charged with growth media supplemented to 15 mM $NaHCO_3$ under 50 μmol photons $\cdot m^{-2} \cdot s^{-1}$ white-light illumination (tungsten incandescent "soft white"). Controlled cultivation was performed using the New Brunswick Bioflo 310 fermentor platform (Eppendorf, Inc., Enfield, CT) equipped with previously described custom-built light-emitting diode (LED) photobioreactor (28). Photobioreactors were operated at a 5.5-liter volume with 250 rpm agitation and main-

tained at 30°C and pH 7.5 (controlled via 2 M NaOH and HCl additions). Scalar incident irradiance (I_i) ranged from 33 to 759 μmol photons $\cdot m^{-2} \cdot s^{-1}$ and combined 680- and 630-nm narrow-band spectra from LED illuminator chips (Marubeni America Corporation, New York, NY). The reactor was sparged at a constant 4.1 liters min^{-1}. In-gas composition was set as a partial nitrogen pressure (pN_2) of 0.98 and a pCO_2 of 0.02 during typical growth conditions; however, O_2 stress conditions were tested by modulating pO_2 from 0 to 0.8 and decreasing pN_2 accordingly. Steady-state biomass concentrations were measured directly as ash-free weight (dry weight) (AFDW) (milligram/liter AFDW) (53) and compared in a standard curve to the indirect OD_{730} measurements obtained using a Genesys 20 visible spectrophotometer (Thermo Scientific, Rockford, IL). Dissolved O_2 concentrations in the reactor was measured with a Clark type O_2 electrode (InPro 6800 series; Mettler Toledo International Inc., Columbus, OH). Physiological steady state was inferred from continuity (≤3% variation between measurements) of the following growth readouts: OD_{730}, pH, and dissolved O_2 concentration. Samples for all the analyses were taken after at least five residence times at steady-state conditions.

Turbidostat control. For turbidostat operation, constant optical densities (OD_{730}) of 0.082 ± 0.003 ($36 \pm 1\ mg_{AFDW}\ liter^{-1}$) were maintained for both cultures across the entire range of irradiances to effectively eliminate self-shading. Incident and transmitted irradiance was measured with six opposing 2π quantum sensors (LI-210SA photometric sensor; LI-COR Biosciences, Lincoln, NE) and intercalibrated with a 4π submerged quantum sensor (LI-193SA spherical underwater quantum sensor; LI-COR Biosciences). Hence, scalar incident irradiance (I_i) is reported here as quanta incident to the center of the reactor and has been confirmed to be both axially and radially isotropic within the liquid culture volume. *In situ* photosynthesis-to-irradiance curves (P-I_i curves) were generated by temporarily stopping flow and subsequently increasing the I_i output of the LEDs over 5-min intervals while concurrently data logging the dissolved O_2 (DO) response within the culture volume (see photosynthesis calculations below).

Microscopic analysis. Microscopic images were acquired on a Zeiss LSM 710 scanning confocal laser microscope (Carl Zeiss MicroImaging GmbH, Jena, Germany) equipped with a W Plan-Apochromatic 63×/1.0 M27 objective. The *Synechococcus* 7002 cells were visualized by phycocyanin autofluorescence measured at 640 nm. Images were processed with Volocity (PerkinElmer, Waltham, MA) and used to obtain the cell size measurements made along the major and minor axis. Cell volumes were calculated using the equation for an ellipsoid, $V = \frac{4}{3}\pi a^2 b$, where a is the diameter of the minor axis and b is the diameter of the major axis.

RNA isolation and sequencing. Cells from a steady-state turbidostat cultures were collected via centrifugation at 7,000 rpm for 5 min at 4°C, flash frozen in liquid nitrogen, and stored at −80°C. Total RNA extraction was performed using standard methodology (54). The quality and integrity of the RNA was assessed on an Agilent 2100 bioanalyzer, and only samples with integrity numbers between 8 and 10 were selected. Template cDNA was prepared using the Applied Biosystems SOLiD total RNA-Seq (transcriptome sequencing) kit (Life Technologies, Carlsbad, CA) according to the manufacturer's protocol. Sequencing was carried out using the SOLiD 5500XL protocol (Life Technologies). The 50-base sequence reads were mapped to the genomes of *Synechococcus* 7002 (GenBank accession number NC_010475), and gene expression levels were determined using the Rockhopper software package as previously described (55). Genes that showed expression values in the bottom 20% of genes at each I_i level for which mRNA was collected were removed from analysis. Hierarchical clustering was performed in the MatLab Bioinformatics Toolbox (MathWorks, Inc.) to identify six distinct profiles of genes with similar expression profiles across irradiance-controlled steady states. Gene expression values (reads per kilobase per million reads [RPKM]) were transformed to log base 2 values and standardized (mean = 0 and standard deviation = 1). Genes in each of the six clusters (profiles) chosen for further analysis

were examined to determine whether certain functions were enriched in a given module. Enrichment is defined as the percentage of genes within the profile for which a function has been assigned being significantly higher than the percentage of genes of the same function in the entire genome with a P value of <0.05 according to Fisher exact test.

Photosynthetic performance. Chl a fluorescence measurements were performed on samples obtained from steady-state turbidostat cultures using pulse amplitude-modulated fluorometry (PAM) in a DUAL-PAM-100 instrument equipped with a photodiode detector and RG665 filter (Walz GmbH, Effeltrich, Germany). Samples were dark adapted for 1 min prior to analyses. Red measuring light (620 nm) was pulsed at the lowest power at 1,000 Hz in the dark and at 10,000 Hz during actinic illumination at 98 μmol photons $\cdot$ m$^{-2} \cdot$ s^{-1} with 635-nm light. Transient fluorescent changes were measured after fluorescence induction through the following: (i) a 200-ms saturating pulse (2,000 μmol photons $\cdot$ m$^{-2} \cdot$ s^{-1}), (ii) 5 s of only far-red light (730 nm), (iii) another 15 s of actinic light, and (iv) 30 s of darkness. The rate of change (rise) of postillumination fluorescence occurring in the dark during step iv results from reduction of plastoquinone (PQ) from NAD(P)H or other reductant accumulated during illumination and was interpreted as a proxy for the rate of cyclic electron transport (rCEF) around PS I (22, 56). Calculations for determining the relative electron transport rates (rETR = PAR $\times \Delta F/F_m'$) have been previously described (57, 58). Rapid light curves were generated by evaluating rETR as a function of increasing PAR values (1-min step intervals). The maximum values and initial slopes (rETR$_{max}$ and α_r, respectively) were determined and interpreted as the relative photosynthetic capacity and relative maximal photosynthetic quantum yield of photochemistry, respectively (58).

Calculations and regression. The net rate of O$_2$ production was calculated from the steady-state mass balance through the bioreactor control volume (equation 1).

$$q_{O_2}x = D\left(\left[O_2^{in}\right] - \left[O_2\right]\right) + k_la\left(k_H pO_2^{in} - \left[O_2\right]\right) \quad (1)$$

The specific rate of O$_2$ production (q_{O_2}) multiplied by the biomass concentration (x) is interpreted here as the net rate of O$_2$ production during photosynthesis (22) and is a function of the dilution rate (D), the lumped mass transfer coefficient (k_la) (0.83 min^{-1}), dissolved O$_2$ concentration ([O$_2$]), and Henry's law partitioning coefficient (k_H = 1.08 mM atm^{-1}). The specific rate of biomass production (q_x; Cmmol biomass hour$^{-1} \cdot$ gram$_{AFDW}^{-1}$) was calculated by assuming the molecular weight of dry biomass to be 24.59 g$_{AFDW} \cdot$ C mol^{-1} (59). Parameterization and curve fitting were performed via nonlinear least-squares regression using the fit function in MatLab with a weighted fit option. All saturating and photoinhibition relationships of growth and photosynthesis were fit with equation 2, where the inhibition index (β) was simplified from the form originally reported by Platt et al. (60) to more clearly represent the theoretical irradiance threshold of inhibition; parameters I_i and I_k are the scalar incident and theoretical saturating irradiances, respectively.

$$R = R_{max}\left[1 - \exp\left(\frac{-I_i}{I_k}\right)\right]\exp\left(\frac{-I_i}{\beta}\right) \quad (2)$$

SUPPLEMENTAL MATERIAL

Supplemental material for this article may be found at http://mbio.asm.org/lookup/suppl/doi:10.1128/mBio.00949-16/-/DCSupplemental.

Figure S1, DOCX file, 0.1 MB.
Figure S2, DOCX file, 0.4 MB.
Table S1, XLSX file, 0.5 MB.
Table S2, XLSX file, 0.3 MB.
Table S3, XLSX file, 0.3 MB.
Table S4, XLSX file, 0.2 MB.
Table S5, XLSX file, 0.2 MB.

REFERENCES

1. **Raven JA.** 2011. The cost of photoinhibition. Physiol Plant **142:**87–104. http://dx.doi.org/10.1111/j.1399-3054.2011.01465.x.
2. **Arnon DI, Whatley FR, Allen MB.** 1954. Photosynthesis by isolated chloroplasts. II. Photosynthetic phosphorylation, the conversion of light into phosphate bond energy. J Am Chem Soc **76:**6324–6329. http://dx.doi.org/10.1021/ja01653a025.
3. **Calvin M, Benson AA.** 1948. The path of carbon in photosynthesis. Science **107:**476–480. http://dx.doi.org/10.1126/science.107.2784.476.
4. **Gubernator B, Bartoszewski R, Kroliczewski J, Wildner G, Szczepaniak A.** 2008. Ribulose-1,5-bisphosphate carboxylase/oxygenase from thermophilic cyanobacterium Thermosynechococcus elongatus. Photosynth Res **95:**101–109. http://dx.doi.org/10.1007/s11120-007-9240-7.
5. **MacKenzie TDB, Campbell DA.** 2005. Cyanobacterial acclimation to rapidly fluctuating light is constrained by inorganic carbon status. J Phycol **41:**801–811. http://dx.doi.org/10.1111/j.1529-8817.2005.00096.x.
6. **Bailey S, Melis A, Mackey KR, Cardol P, Finazzi G, van Dijken G, Berg GM, Arrigo K, Shrager J, Grossman A.** 2008. Alternative photosynthetic electron flow to oxygen in marine *Synechococcus*. Biochim Biophys Acta **1777:**269–276. http://dx.doi.org/10.1016/j.bbabio.2008.01.002.
7. **Raven JA, Larkum AW.** 2007. Are there ecological implications for the proposed energetic restrictions on photosynthetic oxygen evolution at high oxygen concentrations? Photosynth Res **94:**31–42. http://dx.doi.org/10.1007/s11120-007-9211-z.
8. **Vermass WF, Rutherford AW, Hansson O.** 1988. Site-directed mutagenesis in photosystem II of the cyanobacterium *Synechocystis* sp. PCC 6803: donor D is a tyrosine residue in the D2 protein. Proc Natl Acad Sci U S A **85:**8477–8481. http://dx.doi.org/10.1073/pnas.85.22.8477.
9. **Mori T, Binder B, Johnson CH.** 1996. Circadian gating of cell division in cyanobacteria growing with average doubling times of less than 24 hours. Proc Natl Acad Sci U S A **93:**10183–10188. http://dx.doi.org/10.1073/pnas.93.19.10183.
10. **Hagemann M.** 2011. Molecular biology of cyanobacterial salt acclimation. FEMS Microbiol Rev **35:**87–123. http://dx.doi.org/10.1111/j.1574-6976.2010.00234.x.
11. **Burnap RL.** 2015. Systems and photosystems: cellular limits of autotrophic productivity in cyanobacteria. Front Bioeng Biotechnol **3:**1. http://dx.doi.org/10.3389/fbioe.2015.00001.
12. **Molenaar D, van Berlo R, de Ridder D, Teusink B.** 2009. Shifts in growth strategies reflect tradeoffs in cellular economics. Mol Syst Biol **5:**323. http://dx.doi.org/10.1038/msb.2009.82.
13. **Nogales J, Gudmundsson S, Knight EM, Palsson BO, Thiele I.** 2012. Detailing the optimality of photosynthesis in cyanobacteria through systems biology analysis. Proc Natl Acad Sci U S A **109:**2678–2683. http://dx.doi.org/10.1073/pnas.1117907109.
14. **Nogales J, Gudmundsson S, Thiele I.** 2013. Toward systems metabolic engineering in cyanobacteria: opportunities and bottlenecks. Bioengineered **4:**158–163. http://dx.doi.org/10.4161/bioe.22792.
15. **Vu TT, Hill EA, Kucek LA, Konopka AE, Beliaev AS, Reed JL.** 2013. Computational evaluation of *Synechococcus* sp. PCC 7002 metabolism for chemical production. Biotechnol J **8:**619–630. http://dx.doi.org/10.1002/biot.201200315.
16. **Nomura CT, Sakamoto T, Bryant DA.** 2006. Roles for heme–copper oxidases in extreme high-light and oxidative stress response in the cyanobacterium Synechococcus sp. PCC 7002. Arch Microbiol **185:**471–479. http://dx.doi.org/10.1007/s00203-006-0107-7.

17. **Aikawa S, Nishida A, Ho S-H, Chang J-S, Hasunuma T, Kondo A**. 2014. Glycogen production for biofuels by the euryhaline cyanobacteria Synechococcus sp. strain PCC 7002 from an oceanic environment. Biotechnol Biofuels **7**:88. http://dx.doi.org/10.1186/1754-6834-7-88.

18. **Ruffing AM**. 2014. Improved free fatty acid production in cyanobacteria with *Synechococcus* sp. PCC 7002 as host. Front Bioeng Biotechnol **2**:17. http://dx.doi.org/10.3389/fbioe.2014.00017.

19. **Zess EK, Begemann MB, Pfleger BF**. 2016. Construction of new synthetic biology tools for the control of gene expression in the cyanobacterium *Synechococcus* sp. strain PCC 7002. Biotechnol Bioeng **113**:424–432. http://dx.doi.org/10.1002/bit.25713.

20. **Jacobsen JH, Frigaard NU**. 2014. Engineering of photosynthetic mannitol biosynthesis from CO_2 in a cyanobacterium. Metab Eng **21**:60–70. http://dx.doi.org/10.1016/j.ymben.2013.11.004.

21. **Cohen A, Sendersky E, Carmeli S, Schwarz R**. 2014. Collapsing aged culture of the cyanobacterium *Synechococcus elongatus* produces compound(s) toxic to photosynthetic organisms. PLoS One **9**:e100747. http://dx.doi.org/10.1371/journal.pone.0100747.

22. **Beliaev AS, Romine MF, Serres M, Bernstein HC, Linggi BE, Markillie LM, Isern NG, Chrisler WB, Kucek LA, Hill EA, Pinchuk GE, Bryant DA, Wiley HS, Fredrickson JK, Konopka A**. 2014. Inference of interactions in cyanobacterial–heterotrophic co-cultures via transcriptome sequencing. ISME J **8**:2243–2255. http://dx.doi.org/10.1038/ismej.2014.69.

23. **Ludwig M, Bryant DA**. 2012. Synechococcus sp. strain PCC 7002 transcriptome: acclimation to temperature, salinity, oxidative stress, and mixotrophic growth conditions. Front Microbiol **3**:354. http://dx.doi.org/10.3389/fmicb.2012.00354.

24. **Wünschmann G, Brand JJ**. 1992. Rapid turnover of a component required for photosynthesis explains temperature dependence and kinetics of photoinhibition in a cyanobacterium, Synechococcus 6301. Planta **186**:426–433. http://dx.doi.org/10.1007/BF00195324.

25. **Reddy KJ, Haskell JB, Sherman DM, Sherman LA**. 1993. Unicellular, aerobic nitrogen-fixing cyanobacteria of the genus *Cyanothece*. J Bacteriol **175**:1284–1292.

26. **Melnicki MR, Pinchuk GE, Hill EA, Kucek LA, Fredrickson JK, Konopka A, Beliaev AS**. 2012. Sustained H2 production driven by photosynthetic water splitting in a unicellular cyanobacterium. mBio **3**:e00197-12. http://dx.doi.org/10.1128/mBio.00197-12.

27. **Bernstein HC, Kesaano M, Moll K, Smith T, Gerlach R, Carlson RP, Miller CD, Peyton BM, Cooksey KE, Gardner RD, Sims RC**. 2014. Direct measurement and characterization of active photosynthetic zones inside wastewater remediating and biofuel producing microalgal biofilms. Bioresour Technol **156**:206–215. http://dx.doi.org/10.1016/j.biortech.2014.01.001.

28. **Melnicki MR, Pinchuk GE, Hill EA, Kucek LA, Stolyar SM, Fredrickson JK, Konopka AE, Beliaev AS**. 2013. Feedback-controlled LED photobioreactor for photophysiological studies of cyanobacteria. Bioresour Technol **134**:127–133. http://dx.doi.org/10.1016/j.biortech.2013.01.079.

29. **Gilbert M, Wilhelm C, Richter M**. 2000. Bio-optical modelling of oxygen evolution using *in vivo* fluorescence: comparison of measured and calculated photosynthesis/irradiance (PI) curves in four representative phytoplankton species. J Plant Physiol **157**:307–314. http://dx.doi.org/10.1016/S0176-1617(00)80052-8.

30. **MacIntyre HL, Kana TM, Anning T, Geider RJ**. 2002. Photoacclimation of photosynthesis irradiance response curves and photosynthetic pigments in microalgae and cyanobacteria. J Phycol **38**:17–38. http://dx.doi.org/10.1046/j.1529-8817.2002.00094.x.

31. **Sakshaug E, Bricaud A, Dandonneau Y, Falkowski PG, Kiefer DA, Legendre L, Morel A, Parslow J, Takahashi M**. 1997. Parameters of photosynthesis: definitions, theory and interpretation of results. J Plankton Res **19**:1637–1670. http://dx.doi.org/10.1093/plankt/19.11.1637.

32. **Buchanan BB, Schürmann P, Wolosiuk RA, Jacquot J-P**. 2005. The ferredoxin/thioredoxin system: from discovery to molecular structures and beyond, p 859–866. *In* Govindjee, Beatty JT, Gest H, Allen JF (ed), Discoveries in photosynthesis. Springer, Dordrecht, The Netherlands.

33. **Battchikova N, Eisenhut M, Aro EM**. 2011. Cyanobacterial NDH-1 complexes: novel insights and remaining puzzles. Biochim Biophys Acta **1807**:935–944. http://dx.doi.org/10.1016/j.bbabio.2010.10.017.

34. **Imamura S, Asayama M**. 2009. Sigma factors for cyanobacterial transcription. Gene Regul Syst Bio **3**:65–87.

35. **Yu L, Zhao J, Muhlenhoff U, Bryant DA, Golbeck JH**. 1993. PsaE is required for in vivo cyclic electron flow around photosystem I in the cyanobacterium Synechococcus sp. PCC 7002. Plant Physiol **103**:171–180.

36. **Holland SC, Kappell AD, Burnap RL**. 2015. Redox changes accompanying inorganic carbon limitation in *Synechocystis* sp. PCC 6803. Biochim Biophys Acta **1847**:355–363. http://dx.doi.org/10.1016/j.bbabio.2014.12.001.

37. **Schaechter M, Maaloe O, Kjeldgaard NO**. 1958. Dependency on medium and temperature of cell size and chemical composition during balanced growth of *Salmonella typhimurium*. J Gen Microbiol **19**:592–606. http://dx.doi.org/10.1099/00221287-19-3-592.

38. **Constant S, Perewoska I, Alfonso M, Kirilovsky D**. 1997. Expression of the psbA gene during photoinhibition and recovery in Synechocystis PCC 6714: inhibition and damage of transcriptional and translational machinery prevent the restoration of photosystem II activity. Plant Mol Biol **34**:1–13. http://dx.doi.org/10.1023/A:1005754823218.

39. **Huang L, McCluskey MP, Ni H, LaRossa RA**. 2002. Global gene expression profiles of the cyanobacterium Synechocystis sp. strain PCC 6803 in response to irradiation with UV-B and white light. J Bacteriol **184**:6845–6858. http://dx.doi.org/10.1128/JB.184.24.6845-6858.2002.

40. **Kós PB, Deák Z, Cheregi O, Vass I**. 2008. Differential regulation of psbA and psbD gene expression, and the role of the different D1 protein copies in the cyanobacterium Thermosynechococcus elongatus BP-1. Biochim Biophys Acta **1777**:74–83. http://dx.doi.org/10.1016/j.bbabio.2007.10.015.

41. **Sander J, Nowaczyk M, Buchta J, Dau H, Vass I, Deák Z, Dorogi M, Iwai M, Rögner M**. 2010. Functional characterization and quantification of the alternative PsbA copies in Thermosynechococcus elongatus and their role in photoprotection. J Biol Chem **285**:29851–29856. http://dx.doi.org/10.1074/jbc.M110.127142.

42. **Schaefer MR, Golden SS**. 1989. Differential expression of members of a cyanobacterial psbA gene family in response to light. J Bacteriol **171**:3973–3981.

43. **Ludwig M, Bryant DA**. 2011. Transcription profiling of the model cyanobacterium Synechococcus sp. strain PCC 7002 by Next-Gen (SOLiD™) sequencing of cDNA. Front Microbiol **2**:41. http://dx.doi.org/10.3389/fmicb.2011.00041.

44. **Zhu Y, Graham JE, Ludwig M, Xiong W, Alvey RM, Shen G, Bryant DA**. 2010. Roles of xanthophyll carotenoids in protection against photoinhibition and oxidative stress in the cyanobacterium *Synechococcus* sp. strain PCC 7002. Arch Biochem Biophys **504**:86–99. http://dx.doi.org/10.1016/j.abb.2010.07.007.

45. **Mullineaux CW**. 2014. Electron transport and light-harvesting switches in cyanobacteria. Front Plant Sci **5**:7. http://dx.doi.org/10.3389/fpls.2014.00007.

46. **Kramer DM, Avenson TJ, Kanazawa A, Cruz JA, Ivanov B, Edwards GE**. 2004. The relationship between photosynthetic electron transfer and its regulation, p 251–278. *In* Papageorgiou GC, Govindjee (ed), Chlorophyll a fluorescence. A signature of photosynthesis. Springer, Dordrecht, The Netherlands.

47. **Van Liere L, Mur LR**. 1979. Growth kinetics of Oscillatoria agardhii Gomont in continuous culture, limited in its growth by the light energy supply. J Gen Microbiol **115**:153–160. http://dx.doi.org/10.1099/00221287-115-1-153.

48. **Post AF, de Wit R, Mur LR**. 1985. Interactions between temperature and light intensity on growth and photosynthesis of the cyanobacterium Oscillatoria agardhii. J Plankton Res **7**:487–495. http://dx.doi.org/10.1093/plankt/7.4.487.

49. **Lee DY, Rhee G**. 1999. Kinetics of growth and death in *Anabaena flos-aquae* (Cyanobacteria) under light limitation and supersaturation. J Phycol **35**:700–709. http://dx.doi.org/10.1046/j.1529-8817.1999.3540700.x.

50. **Laws EA, Bannister TT**. 1980. Nutrient- and light-limited growth of *Thalassiosira fluviatilis* in continuous culture, with implications for phytoplankton growth in the ocean. Limnol Oceangr **25**:457–473. http://dx.doi.org/10.4319/lo.1980.25.3.0457.

51. **Sakamoto T, Bryant DA**. 2002. Synergistic effect of high-light and low temperature on cell growth of the Δ12 fatty acid desaturase mutant in *Synechococcus* sp. PCC 7002. Photosynth Res **72**:231–242. http://dx.doi.org/10.1023/A:1019820813257.

52. **Stevens S, Patterson C, Myers J**. 1973. The production of hydrogen peroxide by blue-green algae: a survey. J Phycol **9**:427–430.

53. **Pinchuk GE, Hill EA, Geydebrekht OV, De Ingeniis J, Zhang X, Osterman A, Scott JH, Reed SB, Romine MF, Konopka AE, Beliaev AS, Fredrickson JK, Reed JL**. 2010. Constraint-based model of *Shewanella oneidensis* MR-1 metabolism: a tool for data analysis and hypothesis gen-

eration. PLoS Comput Biol **6**:e1000822. http://dx.doi.org/10.1371/journal.pcbi.1000822.

54. **Beliaev AS, Klingeman DM, Klappenbach JA, Wu L, Romine MF, Tiedje JM, Nealson KH, Fredrickson JK, Zhou J**. 2005. Global transcriptome analysis of *Shewanella oneidensis* MR-1 exposed to different terminal electron acceptors. J Bacteriol **187**:7138 –7145. http://dx.doi.org/10.1128/JB.187.20.7138-7145.2005.

55. **McClure R, Balasubramanian D, Sun Y, Bobrovskyy M, Sumby P, Genco CA, Vanderpool CK, Tjaden B**. 2013. Computational analysis of bacterial RNA-Seq data. Nucleic Acids Res **41**:e140. http://dx.doi.org/10.1093/nar/gkt444.

56. **Deng Y, Ye J, Mi H**. 2003. Effects of low CO2 on NAD(P)H dehydrogenase, a mediator of cyclic electron transport around photosystem I in the cyanobacterium Synechocystis PCC6803. Plant Cell Physiol **44**:534 –540. http://dx.doi.org/10.1093/pcp/pcg067.

57. **Sukenik A, Beardall J, Kromkamp J, Kopecký J, Masojídek J, van Bergeijk S, Gabai S, Shaham E, Yamshon A**. 2009. Photosynthetic performance of outdoor *Nannochloropsis* mass cultures under a wide range of environmental conditions. Aquat Microb Ecol **56**:297–308. http://dx.doi.org/10.3354/ame01309.

58. **Schreiber U**. 2004. Pulse-amplitude-modulation (PAM) fluorometry and saturation pulse method: an overview, p 279–319. *In* Papageorgiou GC, Govindjee (ed), Chlorophyll a fluorescence. A signature of photosynthesis. Springer, Dordrecht, The Netherlands.

59. **Roels JA**. 1980. Application of macroscopic principles to microbial metabolism. Biotechnol Bioeng **22**:2457–2514. http://dx.doi.org/10.1002/bit.260221202.

60. **Platt T, Gallegos C, Harrison W**. 1981. Photoinhibition of photosynthesis in natural assemblages of marine phytoplankton. J Mar Res **38**:687–701.